Topological dipole Floquet solitons

Sergey K. Ivanov,[1,2] Yaroslav V. Kartashov,[2,3] Matthias Heinrich,[4] Alexander Szameit,[4] Lluis Torner,[3,5] and Vladimir V. Konotop[6]

[1]*Moscow Institute of Physics and Technology, Institutsky lane 9, Dolgoprudny, Moscow region, 141700, Russia*

[2]*Institute of Spectroscopy, Russian Academy of Sciences, Troitsk, Moscow, 108840, Russia*

[3]*ICFO-Institut de Ciencies Fotoniques, The Barcelona Institute of Science and Technology, 08860 Castelldefels (Barcelona), Spain*

[4]*Institute for Physics, University of Rostock, Albert-Einstein-Str. 23, 18059 Rostock, Germany*

[5]*Universitat Politecnica de Catalunya, 08034, Barcelona, Spain*

[6]*Departamento de Física and Centro de Física Teórica e Computacional, Faculdade de Ciências, Universidade de Lisboa, Campo Grande, Ed. C8, Lisboa 1749-016, Portugal*

We theoretically introduce a new type of topological dipole solitons propagating in a Floquet topological insulator based on a kagome array of helical waveguides. Such solitons bifurcate from two edge states belonging to different topological gaps and have bright envelopes of different symmetries: fundamental for one component, and dipole for the other. The formation of dipole solitons is enabled by unique spectral features of the kagome array which allow the simultaneous coexistence of two topological edge states from different gaps at the same boundary. Notably, these states have equal and nearly vanishing group velocities as well as the same sign of the effective dispersion coefficients. We derive envelope equations describing components of dipole solitons and demonstrate in full continuous simulations that such states indeed can survive over hundreds of helix periods without any noticeable radiation into the bulk.

PhySH Subject Headings: Solitons; Topological insulators, Floquet insulators.

Topological insulators represent a new phase of matter characterized by qualitatively different behavior of excitations in the bulk and at the edge of these topologically nontrivial materials. The phenomenology of topological insulators, originally developed in solid state physics [1,2], was extended to diverse areas of physics, where it stimulated numerous experimental realizations, e.g. in mechanics [3,4], acoustics [5,6], in atomic [7,8], optoelectronic [9-11], and various photonic [12-19] systems. The important progress made in linear topological photonics is described in reviews [20-22], while investigation of topological effects in nonlinear systems is still in its infancy. In such systems evolution of the topological edge states may be considerably affected by nonlinearity and a whole set of novel phenomena, ranging from topologically-protected lasing to the formation of so-called topological edge solitons becomes available [23-25]. Nonlinearity has been shown to impact the modulational stability of topological edge states [26-28], the direction of topological currents [29], the appearance of topologically nontrivial phases [30-32], and to lead to bistability [33]. Furthermore, nonlinearity can give rise to topological closed currents in the bulk of the photonic insulator [34,35] and induce a topological current at its edges [36]. Nonlinear hybridization of topological and bulk states was observed in [37], and the valley Hall effect for vortices in nonlinear system was predicted in [38].

Nonlinearity allows the formation of edge solitons – unique states that exhibit topological protection and simultaneously feature a rich variety of shapes and interactions. Edge solitons were predicted in photonic Floquet insulators in continuous [26,34,39,40] and discrete [41-44] models, and in polariton microcavities [28,45,46]. Their counterparts in nontopological photonic graphene were observed in [47]. Floquet Bragg solitons were reported in [48]. Topological (non-Floquet) systems also allow the formation of Dirac [49], Bragg [50], and valley Hall [51] edge solitons. Even though such states may in principle be encountered in many physical systems, potentially including Bose-Einstein condensates in time-modulated potentials [52,53], only fundamental edge solitons with bell-shaped amplitude profiles have been reported to date. The only exception is Floquet dark-bright states introduced in [40], where opposite signs of the dispersion in two components dictate the dark structure of one of them – nevertheless still representing a fundamental state.

Unlike regular solitons that are rigorously defined, the corresponding concept in nonlinear Floquet insulators refers generically to the observation of localized states in nonlinear topological insulators. Here, by a Floquet soliton (FS) we denote a beam localized in the (x,y)-plane near the interface between topologically different materials, which bears the following two properties: it belongs to a nonlinear family bifurcating from the respective linear Floquet-Bloch edge state, and in the weakly-nonlinear limit its envelope represents a conventional soliton solution of the averaged nonlinear equation with constant coefficients. Due to the broken transversal (in the (x,y)-plane) and longitudinal (along the z-direction) translational symmetries, such states are intrinsically nonstationary, undergoing small-scale oscillations that, as we will see in our numerical simulations, render them effectively metastable, as they decay during evolution albeit remarkably slowly. Thus, the envelopes of FSs analyzed here for a kagome Floquet insulator are described by soliton-bearing coupled nonlinear Schrödinger (NLS) equations with constant coefficients and they remain localized during exceedingly large longitudinal lattice helical periods [26,35].

The *dipole* FSs introduced here are comprised of contributions from *different* topological gaps with envelopes of different symmetries. For the existence of such solitons, the linear edge states they bifurcate from must have equal group velocities and at the same time experience equal *signs* of the dispersions (understood here in terms of the Floquet-Bloch spectrum). Then the system sustains FSs where both components are *bright*. The dipole envelope of the weaker component in such two-dimensional (2D) states is held in shape only by the nonlinear coupling to the stronger fundamental component, as in nontopological vector dipole solitons in uniform media [54-57]. Dipole FSs are hybrid objects that are confined to the edge due to their topological nature, while the nonlinear self-phase modulation enables their localization along the edge. This is in contrast to conventional scalar 2D dipole solitons characterized by identical localization mechanism in two transverse dimensions [58-61].

The propagation of light along the z-axis of a helical kagome array with focusing cubic nonlinearity is governed by the nonlinear

Schrödinger (NLS) equation for the dimensionless field amplitude ψ :

$$i\frac{\partial\psi}{\partial z}=-\frac{1}{2}\Delta_\perp\psi-\mathcal{R}(\mathbf{r},z)\psi-|\psi|^2\psi. \qquad (1)$$

Here $\mathbf{r}=\mathbf{i}x+\mathbf{j}y$ is the radius-vector in the transverse plane, x,y are the normalized transverse coordinates, $\Delta_\perp=\partial^2/\partial x^2+\partial^2/\partial y^2$; z is the normalized propagation distance and the refractive index profile is described by the function $\mathcal{R}(\mathbf{r},z)=\mathcal{R}(\mathbf{r},z+T)=\mathcal{R}(\mathbf{r}+L\mathbf{j},z)$. The array is comprised of identical waveguides of width σ placed in the nodes $\mathbf{r}_{nm}$ of the kagome grid $\mathcal{R}(\mathbf{r},z)=p\sum_{nm}e^{-[\mathbf{r}-\mathbf{r}_{nm}-\mathbf{s}(z)]^2/\sigma^2}$, where p is the array depth, and $\mathbf{s}(z)=r_0(\sin(\omega z),\cos(\omega z)-1)$ describes helical trajectory of each waveguide with the Floquet period $T=2\pi/\omega$ and radius r_0 [Fig. 1(a)]. The y-period of such array is $L=2d$, where d is the separation between waveguides. To obtain edge states, we truncate the array in the x-plane to form zigzag boundaries [Fig. 1(d)]. Typical parameters of such structures are $d\sim1.9$ ($19\ \mu$m spacing), $r_0\sim0.0-1.0$ (helix radius up to $10\ \mu$m), $p\sim12$ (refractive index $\delta n\sim9\times10^{-4}$), $\sigma\sim0.4$ ($4\ \mu$m wide waveguides), $T\sim0-10$ (helix periods up to 12 mm). We assume excitation at $\lambda=800$ nm. Arrays with such parameters can be readily created by femtosecond laser inscription [17]. Notice that topological protection of linear and nonlinear scalar modes in Floquet insulators with helical channels and similar array parameters have already been demonstrated in Refs. [26,40], so we expect the same degree of protection also for dipole vector states analyzed below.

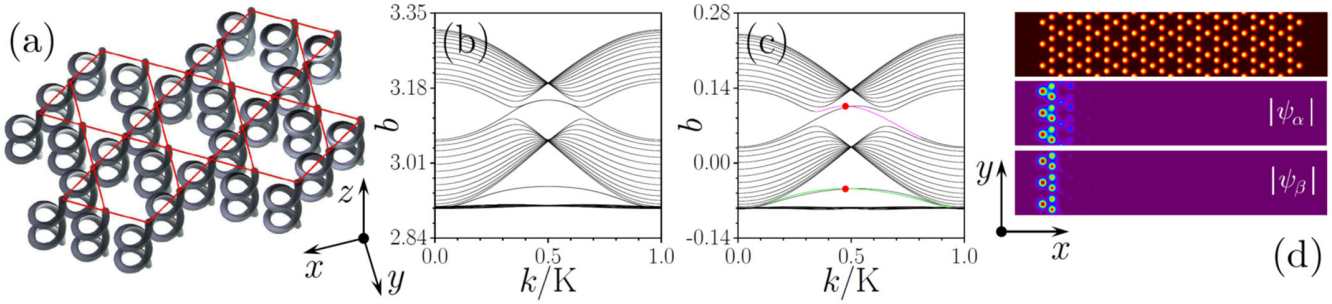

Fig. 1. (a) Schematics of a kagome array of helical waveguides. (b) Dependencies $b(k)$ showing three upper bands from the Bloch spectrum for a finite array [see array profile in Fig. 1(d)] with straight waveguides ($r_0=0$). (c) Quasi-propagation-constants $b(k)$ defined modulo ω for a finite kagome array with helical channels at $r_0=0.6$, $T=8$. Red dots indicate edge states from different gaps with equal velocities $\partial b_{\alpha,\beta}/\partial k$. (d) Three periods of finite kagome array (top) and linear Floquet eigenmodes $\psi_{\alpha,\beta}$ from the left edge (middle and bottom) at $z=0$, $k=0.472\,\mathrm{K}$ corresponding to the red dots in (c). Here and below $p=12$, $d=1.9$, $\sigma=0.4$.

Linear eigenmodes of the helical array are Floquet-Bloch waves $\psi(\mathbf{r},z)=\phi_{\nu k}(\mathbf{r},z)e^{ib_{\nu k}z}$, where $\phi_{\nu k}(\mathbf{r},z)=u_{\nu k}(\mathbf{r},z)e^{iky}$ and the function $u_{\nu k}(\mathbf{r},z)=u_{\nu k}(\mathbf{r},z+T)=u_{\nu k}(\mathbf{r}+L\mathbf{j},z)$ is periodic along both z and y axes. Here k denotes the Bloch momentum in the first Brillouin zone $k\in[-\mathrm{K}/2,+\mathrm{K}/2)$, where $\mathrm{K}=2\pi/L$, ν is the mode index, while $b_{\nu k}\in[-\omega/2,+\omega/2)$ is a quasi-propagation-constant defined modulo ω and describing the phase $b_{\nu k}T$ accumulated by the Floquet-Bloch wave over one z-period. A representative spectrum of a truncated kagome array with straight waveguides (in this case, at $r_0=0$, b is a standard propagation constant) is presented in Fig. 1(b) (for brevity, we omit subscripts in $b_{\nu k}$ in the figures). We show three upper bands, the lowest of which is nearly flat. Two pairs of degenerate edge states are clearly visible in the spectrum. For any non-zero helix radius $r_0\neq0$, the system becomes topologically nontrivial as time-reversal symmetry is broken [62-64]. As a result, topological states occur on the left edge (we assign indices $\nu=\alpha,\beta$ to the "top" and "bottom" states) as marked by magenta and green lines in Fig. 1(c). Representative profiles of Floquet-Bloch waves from different gaps are shown in Fig. 1(d) (at $z=0$).

A remarkable property of the kagome topological insulator is that the derivatives $b'_\nu=\partial b_{\nu k}/\partial k$, defining the group velocities $v_\nu=-b'_\nu$ of two topological states coexisting at a given edge (see [65] for details) may coincide for certain values of the Bloch momentum k [see, e.g. the red dots in Fig. 2(a)]. Importantly, the sign of the dispersion coefficients $b''_\nu=\partial^2 b_{\nu k}/\partial k^2$ for the momentum corresponding to the red dots is likewise identical [Fig. 2(b)]. Coexistence of topological edge states with coinciding group velocities $v_\alpha=v_\beta$ and equal signs of the effective diffraction in the underlying linear system is necessary for the formation of multipole FSs as it allows for persistent nonlinearity-mediated coupling. For our parameters, the group velocities coincide at $k=0.472\,\mathrm{K}$ (see Fig. 2).

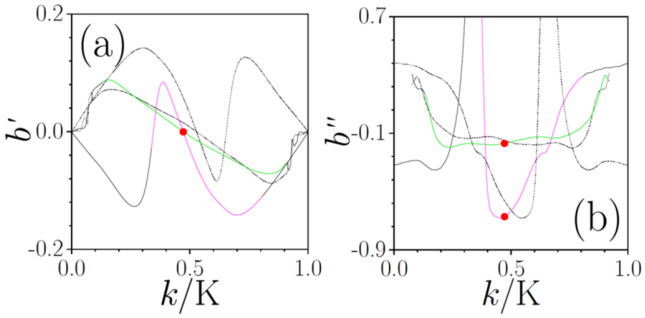

Fig. 2. Derivatives b'_ν (a) and b''_ν (b) for the edge state branches. Solid (dashed) lines correspond to the states from left (right) edges. Red dots indicate states from the left edge with equal group velocities $b'_{\alpha,\beta}=-0.00033$ and negative dispersion $b''_\alpha=-0.67331$, $b''_\beta=-0.16827$ from which FSs bifurcate (see below). The color coding for different branches is the same as in Fig. 1(c).

To construct multipole FSs we focus on their bifurcation from the linear Floquet-Bloch states $\psi_{\alpha k}$ and $\psi_{\beta k}$. To this end we look for the solution in the form $\psi\approx A_\alpha(Y,z)\phi_{\alpha k}e^{ib_{\alpha k}z}+A_\beta(Y,z)\phi_{\beta k}e^{ib_{\beta k}z}$, where $A_{\alpha,\beta}$ are the slowly-varying envelopes and $Y=y-v_{\alpha,\beta}z$ is the coordinate in the frame moving with velocity $v_{\alpha,\beta}=-b'_{\alpha,\beta}$, identical for both components. We adopt a multiscale expansion that shows that the envelopes $A_{\alpha,\beta}$ are governed by the coupled focusing NLS equations [65]:

$$i\frac{\partial A_{\alpha,\beta}}{\partial z}=\frac{b''_{\alpha,\beta}}{2}\frac{\partial^2 A_{\alpha,\beta}}{\partial Y^2}-(\chi_{\alpha,\beta}|A_{\alpha,\beta}|^2+2\chi_x|A_{\beta,\alpha}|^2)A_{\alpha,\beta}, \qquad (2)$$

where $\chi_\nu = \langle(|\phi_{\nu k}|^2, |\phi_{\nu k}|^2)\rangle_T$ and $\chi_x = \langle(|\phi_{\alpha k}|^2, |\phi_{\beta k}|^2)\rangle_T$ are the effective self- and cross-modulation coefficients, averaging over one z-period is defined as $\langle g\rangle_T = T^{-1}\int_0^T g(\mathbf{r}, z)dz$, and calculation of the inner product $(f, g) = \int_S f^*(\mathbf{r}, z)g(\mathbf{r}, z)d\mathbf{r}$ is performed over the entire transverse array area S. Floquet-Bloch states $\phi_{\nu k}$ are orthogonal and normalized at the same instant z [65]: $(\phi_{\nu k}, \phi_{\nu' k}) = \delta_{\nu\nu'}$. Note that the considerable difference between quasi-propagation-constant mismatch $\delta b_k = b_{\alpha k} - b_{\beta k} \approx 0.15$ and frequency of periodic modulation $(\omega \approx 0.78)$ ensures that coupling between the modes is entirely non-resonant and therefore exclusively mediated by nonlinearity. Efficient nonlinear coupling between waves with different momenta k can only occur for special ratio of propagation constants of involved topological states that is not met in our system.

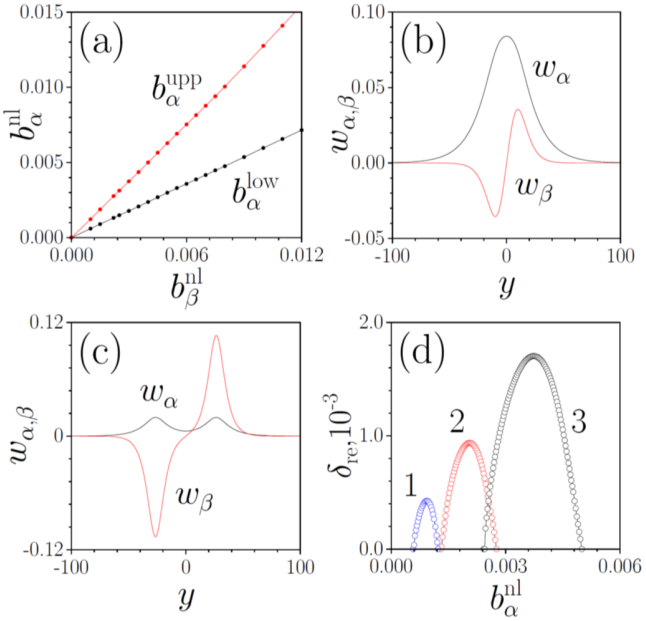

Fig. 3. (a) Domain of dipole soliton existence on the $(b_\alpha^{\rm nl}, b_\beta^{\rm nl})$ plane. Dipole soliton envelopes at $b_\alpha^{\rm nl} = 0.0015$ (b) and $b_\alpha^{\rm nl} = 0.0027$ (c) for $b_\beta^{\rm nl} = 0.0022$. (d) Maximal real part of perturbation growth rate versus $b_\alpha^{\rm nl}$ at $b_\beta^{\rm nl} = 0.001$ (curve 1), 0.0022 (curve 2), and 0.004 (curve 3). The parameters in the envelope equation at $k = 0.472\,\mathrm{K}$ are $b'_\alpha = b'_\beta = -0.00033$, $b''_\alpha = -0.67331$, $b''_\beta = -0.16827$, $\chi_\alpha = 0.31048$, $\chi_\beta = 0.36011$, $\chi_x = 0.31973$.

We are interested in bright dipole soliton solutions of Eqs. (2) that exist at $b''_\alpha, b''_\beta < 0$ [see Fig. 2(b)]. In such states the bell-shaped α component prevents (by creating an effective potential well via cross-phase modulation) out-of-phase poles of the dipole β component from splitting, leading to the formation of stationary states. They can be found by the Newton method in the form $A_{\alpha,\beta} = w_{\alpha,\beta}e^{ib_{\alpha,\beta}^{\rm nl}z}$, where the nonlinearity-induced phase shifts $b_{\alpha,\beta}^{\rm nl}$ should be sufficiently small (much smaller than the quasi-propagation constants, the topological-gap width, and longitudinal Brillouin zone ω) to ensure that the profiles $w_{\alpha,\beta}$ are broad and satisfy the assumption of slow variation of the soliton profile. The properties of dipole solitons for nonlinear and dispersion coefficients corresponding to the edge states at $k = 0.472\,\mathrm{K}$ are described in Fig. 3. For a fixed $b_\beta^{\rm nl}$ dipole solitons exist for $b_\alpha^{\rm low} \le b_\alpha^{\rm nl} \le b_\alpha^{\rm upp}$. The existence domain expands with $b_\beta^{\rm nl}$ [Fig. 3(a)]. Close to its lower border $b_\alpha^{\rm low}$ the dipole β component vanishes and only fundamental α component remains, while at the upper border $b_\alpha^{\rm upp}$ the soliton splits into two states gradually separating as the amplitude of the α component vanishes. Representative profiles are shown in Fig. 3(b) and 3(c). By substituting the perturbed envelope solitons $A_\nu = (w_\nu + \mu_\nu e^{\delta z} + \eta_\nu^* e^{\delta^* z})e^{ib_\nu^{\rm nl}z}$, where $\mu_\nu, \eta_\nu \ll w_\nu$, into Eq. (2) one arrives at a linear eigenvalue problem [65], whose solution yields the growth rate $\delta_{\rm re} = \mathrm{Re}\,\delta$ for the most unstable perturbation depicted in Fig. 3(d) as a function of $b_\alpha^{\rm nl}$. The growth rate $\delta_{\rm re}$ vanishes when $b_\alpha^{\rm nl} \to b_\alpha^{\rm low}, b_\alpha^{\rm upp}$ and for the broad states considered here it remains well below 10^{-3} implying that the characteristic scale $1/\delta_{\rm re}$ of the instability development exceeds hundreds of helix periods T.

To confirm the accuracy of the model (2) and to confirm that topological dipole solitons are observable experimentally, we propagated Floquet-Bloch modes with exact dipole soliton envelopes, obtained from Eq. (2) for various $b_{\alpha,\beta}^{\rm nl}$ values, in the helical kagome array. Such evolution is governed by the full 2D model (1), which we solved with a split-step FFT method. The input for Eq. (1) was constructed as $\psi = w_\alpha(Y)\phi_{\alpha k} + w_\beta(Y)\phi_{\beta k}$. In the right column of Fig. 4(a)-(c) we show (with dots) the modulus of the projections of the field ψ on the linear Floquet-Bloch modes: $c_\nu = \int_{mL-d}^{mL+d} \phi_{\nu k}^*(\mathbf{r}, z)\psi(\mathbf{r}, z)d\mathbf{r}$ ($m \in \mathbb{Z}$ defines the y-period on which projection is calculated), and the input envelopes $w_{\alpha,\beta}$ (solid lines). The projections c_ν explicitly show that dipole soliton at all distances shown contains contributions from two Floquet-Bloch states, whose amplitudes remain practically unchanged and whose envelopes remain mutually localized.

Propagation governed by (1) confirms the metastability of the dipole solitons, which survive over hundreds of helix periods even when small-scale noise (up to 5% in amplitude) is added into the input field distributions. The rotation of the waveguides induces fast z-oscillations of the soliton peak amplitude (a signature of its Floquet nature) and causes very weak radiation, which nevertheless does not destroy the dipole solitons at the considered distances. The weak radiation becomes noticeable only at propagation distances exceeding the ones shown here at least by one order of magnitude. Metastability [associated with very small, but nonzero growth rates $\delta_{\rm re}$ for perturbations in the envelope Eq. (2)] results also in an extremely-slowly growth of the oscillations of the two poles (peaks) of the dipole component (small input noise only slightly affects phase of these oscillations), which nevertheless do not cause splitting of the dipole state at least up to $z < 10^3 T$. Splitting may occur, but at larger distances. The right column of Fig. 4(a)-(c) illustrates the corresponding evolution of the total field ψ. Since the group velocities of the two components are close to zero, the soliton remains virtually locked in place for the parameters chosen above, although for other helix parameters we obtained slowly moving states. If nonlinearity is switched off, wavepackets experience strong diffraction along the array edge at similar propagation distances [Fig. 4(d)], an observation that further confirms that the state from Fig. 4(a)-(c) is sustained by nonlinearity.

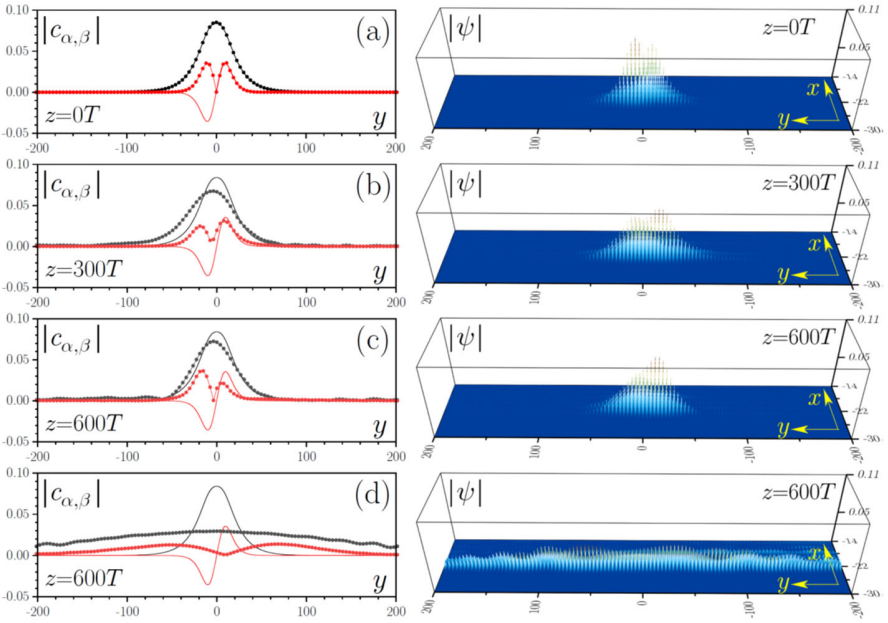

Fig. 4. Propagation of a dipole topological quasi-soliton in Eq. (1) with envelope corresponding to $b_\alpha^{\rm nl}=0.0015$, $b_\beta^{\rm nl}=0.0022$ in the helical kagome array in the nonlinear regime (a)-(c) and its diffraction in the linear regime (d). Left column shows initial envelopes of two components (solid lines) and projections $|c_{\alpha,\beta}|$ at different distances (dots). The right column shows corresponding $|\psi|$ distributions.

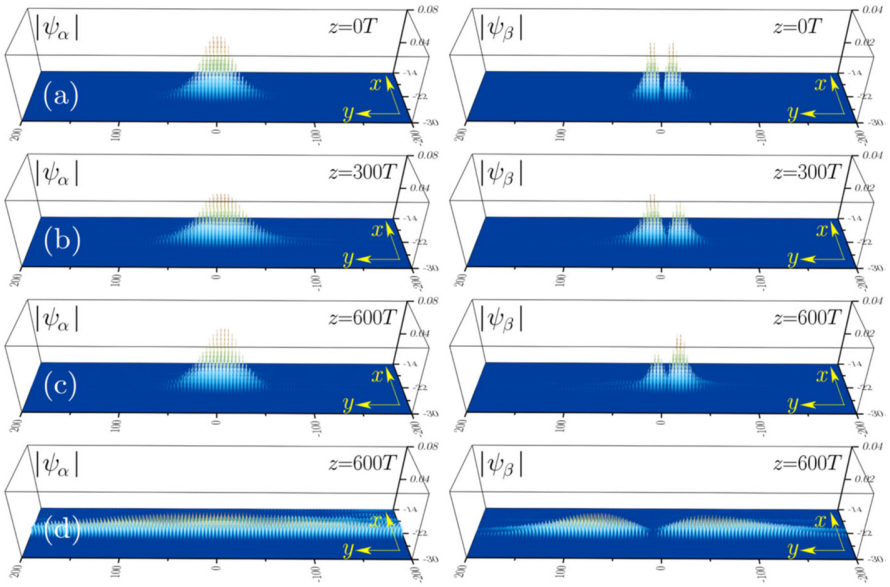

Fig. 5. Propagation of dipole topological quasi-soliton in equivalent vector Eq. (3) in nonlinear medium (a)-(c) and its diffraction in linear regime (d). Left column shows $|\psi_\alpha|$, while right column shows $|\psi_\beta|$. Parameters are the same as in Fig. 4.

When the combination (i.e. total field of the form $\psi\sim\psi_\alpha+\psi_\beta$) of two modes ψ_α and ψ_β with different propagation constants is substituted into (1), one can formally reduce it to two purely nonlinearly coupled 2D NLS equations by collecting terms $\sim e^{ib_{\alpha k}z}, e^{ib_{\beta k}z}$ and dropping oscillating terms $\sim e^{i(b_{\alpha k}-b_{\beta k})z}$ (i.e. accounting only for self- and cross-phase modulation interactions and skipping four-wave mixing terms), without averaging over helix period T:

$$i\frac{\partial\psi_{\alpha,\beta}}{\partial z}=-\frac{1}{2}\Delta_\perp\psi_{\alpha,\beta}-\mathcal{R}(\mathbf{r},z)\psi_{\alpha,\beta}-(|\psi_{\alpha,\beta}|^2+2|\psi_{\beta,\alpha}|^2)\psi_{\alpha,\beta}\quad(3)$$

The advantage of such a reduction is that (3) allows to follow the evolution of each component. This reduction is partially justified due to rapid variation of phase difference $(b_{\alpha k}-b_{\beta k})z$ between modes, but it has to be tested numerically because the scale $(b_{\alpha k}-b_{\beta k})^{-1}>T$ is not the smallest one in the Floquet system. The model (3) can be also directly derived for two waves with different polarizations/wavelengths. The propagation of the dipole FS in the *vector* model (3) with a helical kagome array is illustrated in Fig. 5(a)-(c). Indeed, it shows metastable propagation of the dipole soliton, qualitatively similar to the dynamics encountered in the *scalar* model (Fig. 4). Also, the afore-

mentioned oscillations of the dipole component at the equivalent distances closely match the oscillations of the corresponding projections in Fig. 4 (notice the different direction of the y-axis in panels with projections). As in the scalar model, switching-off nonlinearity causes strong diffraction (see [65] for the evolution of the peak amplitudes in the linear and nonlinear cases). The remarkable similarity between the dynamics in the scalar model (1) and in the vector model (3) shows that the periodic modulation of the array does not introduce any linear coupling of the involved modes.

In conclusion, we uncovered a new type of topological dipole FS, which is constructed using envelopes featuring the different symmetries imposed on two edge states from different topological gaps exhibiting equal group velocities. The solitonic nature of the wavepackets is consistent with their bifurcation from the linear Floquet-Bloch eigenstates at small amplitudes and by the preservation of their shape over extremely long propagation distances. Our prediction has broad implications, as dipole solitons can be observed for other types of Floquet insulators featuring at least two topological gaps, such as, e.g., Floquet Lieb insulators. It is plausible that more complex multicomponent solitons of non-fundamental nature may be also found. Finally, we anticipate that the reported results may be relevant for polaritonic and atomic nonlinear systems, where topological edge solitons can be sustained by different physical mechanisms.

Acknowledgements: Y.V.K. and S.K.I. acknowledge funding of this study by RFBR and DFG according to the research project no. 18-502-12080. A.S. acknowledges funding from the Deutsche Forschungsgemeinschaft (grants BL 574/13-1, SZ 276/19-1, SZ 276/20-1). Y.V.K. and L.T. acknowledge support from the Government of Spain (Severo Ochoa CEX2019-000910-S), Fundació Cellex, Fundació Mir-Puig, Generalitat de Catalunya (CERCA). V.V.K. acknowledges financial support from the Portuguese Foundation for Science and Technology (FCT) under Contract no. UIDB/00618/2020.

References:

1. M. Z. Hasan and C. L. Kane, "Topological insulators," Rev. Mod. Phys. **82**, 3045 (2010).
2. X.-L. Qi and S.-C. Zhang, "Topological insulators and superconductors," Rev. Mod. Phys. **83**, 1057 (2011).
3. R. Süsstrunk and S. D. Huber, "Observation of phononic helical edge states in a mechanical topological insulator," Science **349**, 47 (2015).
4. S. D. Huber, "Topological mechanics," Nat. Phys. **12**, 621 (2016).
5. C. He, X. Ni, H. Ge, X.-C. Sun, Y.-B. Chen, M.-H. Lu, X.-P. Liu, and Y.-F. Chen, "Acoustic topological insulator and robust one-way sound transport," Nat. Phys. **12**, 1124 (2016).
6. Y. G. Peng, C. Z. Qin, D. G. Zhao, Y. X. Shen, X. Y. Xu, M. Bao, H. Jia, and X. F. Zhu, "Experimental demonstration of anomalous Floquet topological insulator for sound," Nat. Commun. **7**, 13368 (2016).
7. G. Jotzu, M. Messer, R. Desbuquois, M. Lebrat, T. Uehlinger, D. Greif, and T. Esslinger, "Experimental realization of the topological Haldane model with ultracold fermions," Nature **515**, 237 (2014).
8. N. Goldman, J. Dalibard, A. Dauphin, F. Gerbier, M. Lewenstein, P. Zoller, and I. B. Spielman, Direct imaging of topological edge states in cold-atom systems, PNAS, **110**, 6736 (2013).
9. A. V. Nalitov, D. D. Solnyshkov, and G. Malpuech, "Polariton Z topological insulator," Phys. Rev. Lett. 114, 116401 (2015).
10. P. St-Jean, V. Goblot, E. Galopin, A. Lemaître, T. Ozawa, L. Gratiet, I. Sagnes, J. Bloch, A. Amo, Lasing in topological edge states of a 1D lattice. Nat. Photon. **11**, 651 (2017).
11. S. Klembt, T. H. Harder, O. A. Egorov, K. Winkler, R. Ge, M. A. Bandres, M. Emmerling, L. Worschech, T. C. H. Liew, M. Segev, C. Schneider, and S. Höfling, Exciton-polariton topological insulator, Nature **562**, 552 (2018).
12. F. D. Haldane and S. Raghu, "Possible realization of directional optical waveguides in photonic crystals with broken time-reversal symmetry," Phys. Rev. Lett. **100**, 013904 (2008).
13. Z. Wang, Y. Chong, J. D. Joannopoulos, and M. Soljacic, "Observation of unidirectional backscattering-immune topological electro-magnetic states," Nature **461**, 772 (2009).
14. M. Hafezi, E. A. Demler, M. D. Lukin, and J. M. Taylor, "Robust optical delay lines with topological protection," Nat. Phys. **7**, 907 (2011).
15. A. B. Khanikaev, S. H. Mousavi, W. K. Tse, M. Kargarian, A. H. MacDonald, G. Shvets, "Photonic topological insulators," Nat. Materials **12**, 233 (2013).
16. N. H. Lindner, G. Refael, and V. Galitski, "Floquet topological insulator in semiconductor quantum wells," Nat. Phys. **7**, 490 (2011).
17. M. C. Rechtsman, J. M. Zeuner, Y. Plotnik, Y. Lumer, D. Podolsky, F. Dreisow, S. Nolte, M. Segev, and A. Szameit, "Photonic Floquet topological insulators," Nature **496**, 196 (2013).
18. L. J. Maczewsky, J. M. Zeuner, S. Nolte, and A. Szameit, "Observation of photonic anomalous Floquet topological insulators," Nat. Commun. **8**, 13756 (2017).
19. S. Mukherjee, A. Spracklen, M. Valiente, E. Andersson, P. Öhberg, N. Goldman, R. R. Thomson, "Experimental observation of anomalous topological edge modes in a slowly driven photonic lattice," Nat. Commun. **8**, 13918 (2017).
20. L. Lu, J. D. Joannopoulos, and M. Soljačić, "Topological photonics," Nat. Photon. **8**, 821 (2014).
21. T. Ozawa, H. M. Price, A. Amo, N. Goldman, M. Hafezi, L. Lu, M. C. Rechtsman, D. Schuster, J. Simon, O. Zilberberg, I. Carusotto, "Topological photonics," Rev. Mod. Phys. **91**, 015006 (2019).
22. M. Kim, Z. Jacob, and J. Rho, "Recent advances in 2D, 3D and higher-order topological photonics," Light: Science & Applications **9**, 130 (2020).
23. D. Smirnova, D. Leykam, Y. D. Chong, and Y. Kivshar, "Nonlinear topological photonics," Appl. Phys. Rev. **7**, 021306 (2020).
24. Y. Ota, K. Takata, T. Ozawa, A. Amo, Z. Jia, B. Kante, M. Notomi, Y. Arakawa, S. Iwamoto, "Active topological photonics," Nanophotonics **9**, 547 (2020).
25. S. Rachel, Interacting topological insulators: A review. Reports Prog. Phys. **81**, 116501 (2018).
26. D. Leykam and Y. D. Chong, "Edge solitons in nonlinear-photonic topological insulators", Phys. Rev. Lett. 117, 143901 (2016).
27. Y. Lumer, M. C. Rechtsman, Y. Plotnik, and M. Segev, "Instability of bosonic topological edge states in the presence of interactions," Phys. Rev. A 94, 021801(R) (2016).
28. Y. V. Kartashov and D. V. Skryabin, "Modulational instability and solitary waves in polariton topological insulators," Optica **3**, 1228 (2016).
29. O. Bleu, D. D. Solnyshkov, and G. Malpuech, "Interacting quantum fluid in a polariton Chern insulator," Phys. Rev. B **93**, 085438 (2016).
30. Y. Hadad, J. C. Soric, A. B. Khanikaev, and A. Alú, "Self-induced topological protection in nonlinear circuit arrays," Nat. Electron. **1**, 178 (2018).
31. Y. Hadad, A. B. Khanikaev, and A. Alù, "Self-induced topological transitions and edge states supported by nonlinear staggered potentials," Phys. Rev. B **93**, 155112 (2016).
32. F. Zangeneh-Nejad, R. Fleury, "Nonlinear second-order topological insulators," Phys. Rev. Lett. **123**, 053902 (2019).
33. Y. V. Kartashov, D. V. Skryabin, "Bistable topological insulator with exciton-polaritons," Phys. Rev. Lett. **119**, 253904 (2017).
34. Y. Lumer, Y. Plotnik, M. C. Rechtsman, and M. Segev, "Self-localized states in photonic topological insulators," Phys. Rev. Lett. **111**, 243905 (2013).

35. S. Mukherjee and M. C. Rechtsman, "Observation of Floquet solitons in a topological bandgap," Science **368**, 856 (2020).
36. L. J. Maczewsky, M. Heinrich, M. Kremer, S. K. Ivanov, M. Ehrhardt, F. Martinez, Y. V. Kartashov, V. V. Konotop, L. Torner, D. Bauer, and A. Szameit, "Nonlinearity-induced photonic topological insulator," Science **370**, 701 (2020).
37. D. Dobrykh, A. Yulin, A. Slobozhanyuk, A. Poddubny, and Y. Kivshar, "Nonlinear control of electromagnetic topological edge states," Phys. Rev. Lett. **121**, 163901 (2018).
38. O. Bleu, G. Malpuech, D. D. Solnyshkov, "Robust quantum valley Hall effect for vortices in an interacting bosonic quantum fluid," Nat. Commun. **9**, 3991 (2018).
39. S. K. Ivanov, Y. V. Kartashov, L. J. Maczewsky, A. Szameit, V. V. Konotop, "Edge solitons in Lieb topological Floquet insulator," Opt. Lett. **45**, 1459 (2020).
40. S. K. Ivanov, Y. V. Kartashov, A. Szameit, L. Torner, V. V. Konotop, "Vector topological edge solitons in Floquet insulators," ACS Photonics **7**, 735 (2020).
41. M. J. Ablowitz, C. W. Curtis, and Y.-P. Ma, "Linear and nonlinear traveling edge waves in optical honeycomb lattices," Phys. Rev. A **90**, 023813 (2014).
42. M. J. Ablowitz and J. T. Cole, "Tight-binding methods for general longitudinally driven photonic lattices: Edge states and solitons," Phys. Rev. A 96, 043868 (2017).
43. M. J. Ablowitz and Y. P. Ma, "Strong transmission and reflection of edge modes in bounded photonic graphene," Opt. Lett. 40, 4635 (2015).
44. A. Bisianov, M. Wimmer, U. Peschel, and O. A. Egorov, "Stability of topologically protected edge states in nonlinear fiber loops", Phys. Rev. A **100**, 063830 (2019).
45. D. R. Gulevich, D. Yudin, D. V. Skryabin, I. V. Iorsh, and I. A. Shelykh, "Exploring nonlinear topological states of matter with exciton-polaritons: Edge solitons in kagome lattice," Sci. Rep. **7**, 1780 (2017).
46. C. Li, F. Ye, X. Chen, Y. V. Kartashov, A. Ferrando, L. Torner, D. V. Skryabin, "Lieb polariton topological insulators," Phys. Rev. B **97**, 081103 (R) (2018).
47. Z. Zhang, R. Wang, Y. Zhang, Y. V. Kartashov, F. Li, H. Zhong, H. Guan, K. Gao, F. Li, Y. Zhang, M. Xiao, "Observation of edge solitons in photonic graphene," Nat. Commun. **11**, 1902 (2020).
48. S. K. Ivanov, Y. V. Kartashov, L. J. Maczewsky, A. Szameit, V. V. Konotop, "Bragg solitons in topological Floquet insulators," Opt. Lett. **45**, 2271 (2020).
49. D. A. Smirnova, L. A. Smirnov, D. Leykam, and Y. S. Kivshar, "Topological edge states and gap solitons in the nonlinear Dirac model," Las. Photon. Rev. **13**, 1900223 (2019).
50. W. Zhang, X. Chen, and Y. V. Kartashov, V. V, Konotop, and F. Ye, "Coupling of Edge States and Topological Bragg Solitons," Phys. Rev. Lett. **123**, 254103 (2019).
51. H. Zhong, S. Xia, Y. Li, Y. Zhang, D. Song, C. Liu, and Z. Chen, "Nonlinear Topological Valley Hall Edge States Arising from Type-II Dirac Cones", arXiv:2010.02902.
52. Focus on topological physics: from condensed matter to cold atoms and optics, H. Zhai, M. Rechtsman, Y.-M. Lu, and K. Yang (Eds), New J. Phys. **18** (2016).
53. M. S. Rudner, N. H. Lindner, "Band structure engineering and non-equilibrium dynamics in Floquet topological insulators," Nat. Rev. Phys. **2**, 229 (2020).
54. D. N. Christodoulides and R. J. Joseph, "Vector solitons in birefringent nonlinear dispersive media," Opt. Lett. **13**, 53 (1988).
55. M. Mitchell, M. Segev, D. N. Christodoulides, "Observation of multihump multimode solitons," Phys. Rev. Lett. **80**, 4657 (1998).
56. J. J. García-Ripoll, V. M. Pérez-García, E. A. Ostrovskaya, and Y. S. Kivshar, "Dipole-mode vector solitons," Phys. Rev. Lett. **85**, 82 (2000).
57. W. Krolikowski, E. A. Ostrovskaya, C. Weilnau, M. Geisser, G. McCarthy, Y. S. Kivshar, C. Denz, and B. Luther-Davies, "Observation of dipole-mode vector solitons," Phys. Rev. Lett. **85**, 1424 (2000).
58. J. Yang, I. Makasyuk, A. Bezryadina, Z. Chen, "Dipole solitons in optically induced two-dimensional photonic lattices," Opt. Lett. **29**, 1662 (2004).
59. Y. V. Kartashov, A. A. Egorov, L. Torner, D. N. Christodoulides, "Stable soliton complexes in two-dimensional photonic lattices," Opt. Lett. **29**, 1918 (2004).
60. F. Lederer, G. I. Stegeman, D. N. Christodoulides, G. Assanto, M. Segev, Y. Silberberg, "Discrete Solitons in Optics," Phys. Rep. **463**, 1 (2008).
61. Y. V. Kartashov, V. A. Vysloukh, L. Torner, "Soliton shape and mobility control in optical lattices," Prog. Opt. **52**, 63 (2009).
62. M. S. Rudner, N. H. Lindner, E. Berg, M. Levin, "Anomalous edge states and the bulk-edge correspondence for periodically driven two-dimensional systems," Phys. Rev. X 3, 031005 (2014).
63. H. Zhong, R. Wang, F. W. Ye, J. W. Zhang, L. Zhang, Y. P. Zhang, M. R. Belic, and Y. Q. Zhang, "Topological insulator properties of photonic kagome helical waveguide arrays," Results in Physics **12**, 996 (2019).
64. M. J. Ablowitz and J. T. Cole, "Topological insulators in longitudinally driven waveguides: Lieb and kagome lattices," Phys. Rev. A 99, 033821 (2019).
65. See Supplemental Material for derivation of the envelope equations, and details of the linear stability analysis.
66. Y. S. Kivshar, G. P. Agrawal, Optical Solitons: From Fibers to Photonic Crystals (Academic Press, New York, 2003).